Journal of Materials Science and Chemical Engineering, 2026, 14(8), 58-82
https://www.scirp.org/journal/msce
ISSN Online: 2327-6053
ISSN Print: 2327-6045

Multi-Scale Chemo-Mechanical Modeling of Eco-Self-Compacting Concrete Incorporating Recycled Glass Powder

Maingha Ronald Rigain[1*], Odi Enyegue Thierry[1], Langola Olivier[1], Abanda André[1], Kenmogne Fabien[2], Kikmo Wilba Christophe[1], Koffi Djanna Francis Lénine[3]

[1]National Higher Polytechnic School of Douala, University of Douala, Douala, Cameroon
[2]Department of Civil Engineering, Advanced Technical Teacher Training College of Technical Education, University of Douala, Douala, Cameroon
[3]Technologies and Applied Sciences Laboratory, University Institute of Technology of Douala, University of Douala, Douala, Cameroon
Email: *maingharonalddrigain@gmail.com

How to cite this paper: Rigain, M.R., Thierry, O.E., Olivier, L., André, A., Fabien, K., Christophe, K.W. and Lénine, K.D.F. (2026) Multi-Scale Chemo-Mechanical Modeling of Eco-Self-Compacting Concrete Incorporating Recycled Glass Powder. *Journal of Materials Science and Chemical Engineering*, **14**, 58-82.
https://doi.org/10.4236/msce.2026.148004

Received: February 23, 2026
Accepted: August 14, 2026
Published: August 17, 2026

Abstract

We present a mechanistic multiscale framework for the joint analysis of mechanical performance and durability of eco-designed self-compacting concrete incorporating recycled glass powder. At the microscale, the cementitious matrix is described as a hierarchical composite comprising calcium-silicate-hydrate (C-S-H), portlandite (CH), and finely ground glass, with explicit physico-chemical interactions between these phases. The pozzolanic reactivity of the glass is modeled by a kinetic law that links the local consumption of portlandite to the specific surface area of the glass particles, thereby inducing controlled microstructural densification and an evolution of the connected porosity. On the mechanical side, an operator-based homogenization scheme of Mori-Tanaka type relates the effective elasticity tensor to the intrinsic properties of the constituent phases and to the glass volume fraction. On the transport side, durability is addressed through a diffusion-reaction model in which the effective diffusivity depends explicitly on the evolving porosity, thus capturing the permeability reduction induced by the pozzolanic reaction. These ingredients are coupled into a multiphysics-multiscale system in which the glass volume fraction ϕ_g appears as a design parameter. The precise mathematical problem considered is the characterization of an optimal glass content through an objective functional $F(\phi_g) = \alpha E_{\text{eff}}(\phi_g) - \beta D_{\text{eff}}(\phi_g)$, which balances effective stiffness E_{eff} against effective diffusivity D_{eff} for prescribed positive weights α, β. Under explicit structural assumptions on

the maps $\phi_g \mapsto E_{\text{eff}}(\phi_g)$ and $\phi_g \mapsto D_{\text{eff}}(\phi_g)$ (monotonicity, concavity/convexity, and endpoint behaviour), we prove that F is strictly concave on the admissible interval $[0, \phi_{\text{crit}}]$ and admits a unique critical point $\phi_g^{\text{opt}} \in (0, \phi_{\text{crit}})$, which is the unique global maximizer of F. This result establishes, in a mathematically precise sense, the existence and uniqueness of an optimal recycled glass volume fraction that achieves a well-defined trade-off between mechanical reinforcement and mitigation of diffusive degradation. Numerical simulations of the coupled chemo-microstructural-transport-mechanical problem illustrate the qualitative behaviour predicted by the analysis and exhibit the same optimality structure, thereby providing a coherent numerical counterpart to the theoretical result. Beyond its intrinsic predictive capabilities, the proposed model offers a structured, operator-based formulation that can serve both as a tool for the rational design of sustainable concretes and as a physics-based prior in data-driven frameworks. In particular, the governing equations and homogenized operators can be embedded as constraints or inductive biases in transfer-learning or domain-adaptation settings, and the effective laws $D_{\text{eff}}(\phi_p)$ and $\mathbb{C}^{\text{eff}}(\phi_p)$ constitute natural targets for interpretable surrogate models constructed via symbolic regression, explainable machine learning, or Kolmogorov-Arnold-type networks. This opens a pathway toward quantitatively reliable, computationally efficient, and physically consistent design tools for next-generation eco-efficient cementitious composites, and provides a clear roadmap for integrating future experimental calibration and hybrid computational strategies to obtain quantitative predictions for $C_{CH}(t)$, $\phi_p(t)$, $D_{\text{eff}}(t)$, and $E_{\text{eff}}(t)$.

Keywords

Multiscale Modeling, Chemo-Mechanical Coupling, Recycled Glass Powder, Durability of Cementitious Materials, Homogenization, Physics-Informed Surrogates, Optimization of Composite Microstructures

1. Introduction

The transition toward sustainable civil engineering materials has become a central scientific and technological challenge. Among the most pressing issues are the efficient valorization of industrial and municipal wastes and the reduction of the carbon footprint associated with cement production, which remains one of the largest contributors to global anthropogenic CO_2 emissions [1] [2]. In this context, the incorporation of recycled glass powder into cementitious matrices has emerged as a promising strategy for producing environmentally friendly concretes while simultaneously diverting large quantities of glass waste from landfills.

A substantial body of experimental research has demonstrated that finely ground glass powder can exhibit significant pozzolanic reactivity, leading to the consumption of portlandite and the formation of additional calcium silicate hy-

drates (C-S-H). These reactions may enhance microstructural compactness, improve long-term durability, and modify the mechanical behavior of the composite material. Nevertheless, despite these advances, most existing modeling approaches remain essentially empirical or semi-empirical. Such formulations typically rely on regression-based relationships calibrated for specific mixture compositions and curing conditions, which significantly limits their predictive capability when extrapolating to new materials, glass waste streams, or environmental conditions [3] [4].

In parallel, recent years have witnessed the rapid development of *data-driven* and hybrid computational strategies for the design and optimization of cementitious materials incorporating recycled glass powder. Machine-learning-assisted mix design methods have demonstrated the capacity to explore large compositional spaces and to simultaneously optimize mechanical strength, economic cost, and environmental indicators such as CO_2 emissions. For example, recent studies on machine-learning-assisted sustainable mix design of waste glass powder concrete have shown that predictive algorithms can identify optimal trade-offs between strength, cost, and carbon footprint across extensive datasets of experimental mixtures. Similarly, integrated prediction frameworks combining synthetic data augmentation techniques—such as generative adversarial models with stacked machine learning architectures have been proposed to improve predictive robustness for recycled concrete properties, particularly in situations where experimental data are scarce.

Despite their remarkable predictive efficiency, purely data-driven models often suffer from a lack of physical interpretability and may struggle to extrapolate reliably beyond the domain of their training data. This limitation becomes particularly critical when addressing long-term durability phenomena, novel glass waste compositions, or extreme environmental exposure conditions. In contrast, physics-based mechanistic models explicitly encode the governing laws of chemical reactions, transport processes, and mechanical interactions. Such models offer deeper insight into the causal mechanisms governing material behavior and provide a more reliable framework for extrapolation to unexplored scenarios. Consequently, data-driven and mechanistic approaches should be regarded as complementary rather than competing paradigms: machine learning techniques can accelerate parameter identification or surrogate modeling, whereas mechanistic formulations establish physically grounded predictive frameworks.

Nevertheless, several fundamental scientific challenges remain unresolved. First, the current literature lacks a unified theoretical framework capable of consistently coupling the chemical kinetics of pozzolanic reactions with microstructural evolution, multiphysics transport phenomena, and macroscopic mechanical behavior. Most existing models treat these processes separately or rely on simplified empirical relationships that do not capture their strong mutual interactions. Second, mechanical homogenization approaches applied to cementitious composites are often restricted to a single structural scale, preventing a detailed representation of hierarchical phase interactions between micro- and meso-scale constituents. Third, durability models based on diffusion equations generally neglect

the dynamic evolution of pore structure induced by pozzolanic reactions, thereby limiting their ability to predict the time-dependent evolution of permeability and transport properties [5] [6].

From a theoretical perspective, another important question remains largely unexplored: the existence of an optimal volumetric fraction of recycled glass powder capable of simultaneously maximizing mechanical reinforcement and minimizing the diffusivity of aggressive species. Although experimental studies frequently report optimal replacement levels within restricted ranges, these observations remain largely empirical and lack a rigorous mathematical justification derived from the underlying multi-physics interactions governing the composite material.

To address these limitations, the present study develops a unified mechanistic multi-scale framework for eco-designed self-compacting concrete incorporating recycled glass powder. The proposed formulation explicitly couples pozzolanic reaction kinetics with microstructural evolution through porosity reduction, integrates multiphysics transport processes governing the diffusion of aggressive chemical species, and employs a generalized Mori-Tanaka homogenization scheme to characterize the effective mechanical properties of the evolving heterogeneous composite [6]-[8].

Beyond the formulation of the coupled chemo-mechanical model, the present work also establishes a rigorous mathematical analysis demonstrating the existence of an optimal glass powder volumetric fraction arising from the competition between mechanical reinforcement and diffusivity reduction mechanisms. This theoretical result provides a fundamental insight into the rational design of sustainable cementitious composites and represents, to the best of the authors' knowledge, one of the first formal demonstrations of such an optimum within a fully coupled multi-scale chemo-mechanical framework. Through the integration of chemical kinetics, transport phenomena, mechanical homogenization, and mathematical analysis, this work aims to establish a coherent theoretical foundation capable of guiding the rational design of high-performance and environmentally sustainable self-compacting concretes incorporating recycled glass powder.

2. Material Characterization and Morphological Parameters

The predictive capability of the proposed chemo-mechanical multi-scale framework strongly depends on a rigorous characterization of the recycled glass powder incorporated into the cementitious matrix. In particular, particle morphology, particle size distribution, chemical composition, and specific surface area directly control the kinetics of glass dissolution, the development of secondary hydration products, and the evolution of transport properties within the hardened material. Consequently, the experimental characterization presented in this section is not purely descriptive. It provides the quantitative parameters that explicitly enter the kinetic, mechanical homogenization, and transport equations introduced in the subsequent sections of the model.

2.1. Origin and Typology of Recycled Glass

The recycled glass considered in this work originates primarily from post-consumer soda-lime container glass collected from municipal recycling facilities. Container glass constitutes one of the most abundant and chemically stable sources of recyclable silica-rich materials and is therefore widely considered suitable for pozzolanic applications in cementitious systems [7] [9] [10].

More generally, several categories of recycled glass can be distinguished according to their industrial origin and chemical composition:

- **Container glass**: obtained from recycled bottles and jars. This glass represents the main source used in the present study due to its availability and relatively homogeneous soda-lime composition.
- **Flat glass**: originating from building and automotive glazing. Its homogeneous composition and smooth surface also make it suitable for grinding into fine powders.
- **Tempered glass**: thermally treated glass characterized by high mechanical strength, whose recycling into powder is more complex due to its fragmentation behavior.
- **Technical glasses**: including borosilicate or electronic glasses with specialized chemical compositions that generally limit their use in cementitious systems.

After collection, the container glass undergoes a standardized processing sequence including sorting, impurity removal, washing, and controlled mechanical grinding. The resulting powder is then sieved to obtain a controlled particle size distribution compatible with the rheological requirements of self-compacting concrete.

Figure 1 illustrates representative stages of the recycling and preparation process.

2.2. Morphological and Microstructural Analysis

The morphology of the ground glass particles is investigated using optical microscopy and scanning electron microscopy (SEM). These techniques provide detailed information on particle size distribution, particle angularity, and surface roughness, which are critical parameters governing both mechanical interlocking and chemical reactivity within the cementitious matrix [11].

The observations reveal that the grinding process generates particles with predominantly angular geometry and irregular surfaces. Such angularity enhances mechanical interlocking between particles and the surrounding cement paste, thereby improving stress transfer at the microscale.

The particle size distribution obtained after sieving is centered approximately in the range 5 - 80 μm, which is comparable to that of Portland cement particles. This granulometric compatibility promotes homogeneous dispersion of the glass powder within the cementitious matrix and contributes to improved packing density in self-compacting concrete mixtures.

Representative micrographs illustrating these morphological characteristics are presented in Figure 2.

(a) Container glass collected from recycling facilities. (b) Cleaning and preparation stages prior to grinding.

Figure 1. Preparation process of recycled container glass used for powder production.

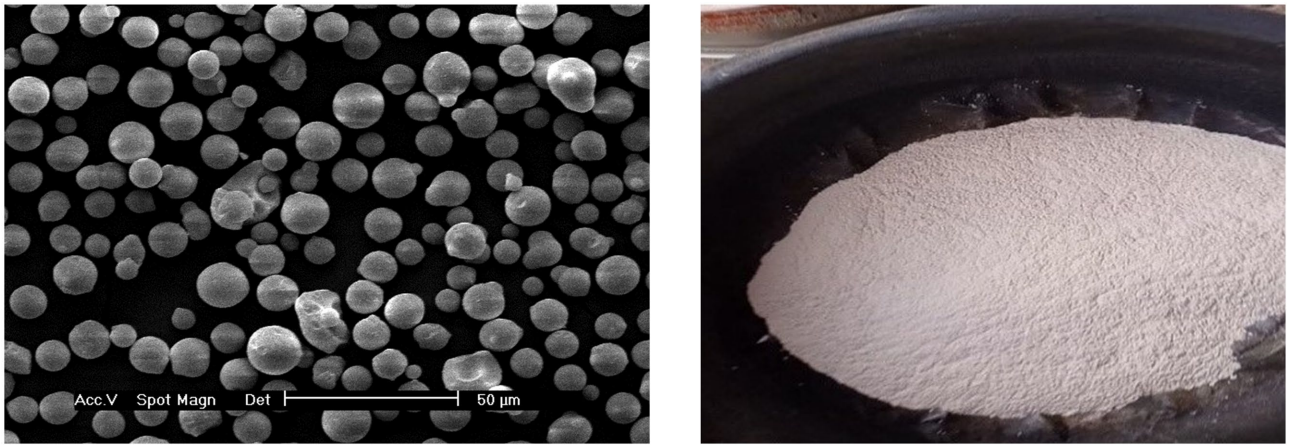

(a) Optical microscopy illustrating particle size distribution.

(b) SEM micrograph highlighting angular morphology and surface roughness.

Figure 2. Morphological features of recycled glass powder used in this study.

Beyond their descriptive role, these observations are used to calibrate the particle shape factor and to define representative particle size classes introduced in the kinetic and transport formulations of the model.

2.3. Specific Surface Area and Implications for Reaction Kinetics

The specific surface area of the glass powder is determined using the Brunauer-Emmett-Teller (BET) adsorption method. The measured values typically range

between 1 and 5 $m^2 g^{-1}$, depending on grinding fineness and particle size distribution, which is consistent with values reported in the literature for finely ground recycled glass powders [12] [13].

In the kinetic framework adopted in this work, the specific surface area directly controls the reactive surface available for alkaline dissolution. The specific glass surface per unit volume of composite is expressed as $a_g = \rho_g S_{BET} \phi_g$, where ρ_g denotes the true density of glass and ϕ_g its volumetric fraction in the composite [13] [14].

The dissolution rate of the glass phase is therefore modeled as $R_{diss} = k_{diss} a_g f(\mathrm{pH}, T)$, where k_{diss} is the intrinsic dissolution constant and $f(\mathrm{pH}, T)$ represents the influence of pore solution alkalinity and temperature.
This formulation explicitly links the experimentally measured BET surface area to the temporal evolution of the reactive glass fraction.

2.4. Physico-Chemical Properties

Chemical composition: X-ray fluorescence (XRF) analyses indicate that the recycled glass is predominantly composed of amorphous silica (SiO_2), with typical concentrations exceeding 70%. Secondary oxides such as Na_2O, CaO, and minor quantities of Al_2O_3 are also present, reflecting the classical composition of soda-lime glass [15]. The high proportion of amorphous silica provides a source of reactive silica capable of participating in pozzolanic reactions with portlandite, leading to the formation of additional C-S-H phases [16].

Density and volumetric parameters: The true density of the glass powder, measured by helium pycnometry, is approximately 2.45 g cm^{-3}, slightly lower than that of Portland cement. This parameter is explicitly incorporated into the computation of volumetric fractions and subsequently used in the Mori-Tanaka homogenization scheme adopted for the mechanical modeling.

Implications for transport processes: The progressive dissolution of glass particles and the precipitation of secondary hydration products induce a densification of the cementitious microstructure and a reduction of connected porosity. These microstructural transformations significantly influence the transport properties of the material.

Within the transport model proposed in this study, the effective diffusion coefficient of aggressive species is expressed as $D_{\mathrm{eff}}(t) = D_0 \phi(t)^n$, where $\phi(t)$ denotes the evolving porosity controlled by pozzolanic reaction kinetics. Through the coupling between dissolution kinetics, surface area, and porosity evolution, the experimentally measured morphological parameters therefore directly influence the predicted durability of the cementitious composite [15] [17].

Overall, the characterization presented in this section provides the quantitative morpho-physico-chemical parameters required for the subsequent multi-scale modeling framework. In particular, the particle size distribution, BET specific surface area, and glass volumetric fraction constitute key inputs for the coupled kinetic, mechanical homogenization, and transport equations governing the chemo-

mechanical behavior of the proposed eco-designed self-compacting concrete.

3. Material Description and Multi-Scale Framework

This section introduces the theoretical framework used to describe the chemo-mechanical behaviour of cementitious composites incorporating recycled glass powder. The formulation relies on a rigorous multi-scale approach in which chemical kinetics, microstructural evolution, transport processes and mechanical homogenization are consistently coupled. The objective of this framework is to establish a physically consistent and mathematically well-posed representation of the material behaviour across scales, linking microscopic reaction mechanisms to the effective macroscopic properties governing durability and structural performance.

3.1. Fundamental Modelling Assumptions

The multi-scale formulation is constructed under a set of structural assumptions ensuring both physical relevance and analytical tractability.

(i) Separation of spatial scales. The characteristic size of the microstructural heterogeneities (glass particles, hydration products and pores) is assumed to be much smaller than the macroscopic structural scale. This hypothesis allows the introduction of a small asymptotic parameter $\varepsilon \ll 1$, defined as the ratio between microscopic and macroscopic length scales. This assumption provides the mathematical basis for asymptotic homogenization.

(ii) Statistical homogeneity of the microstructure. At the mesoscale, the composite exhibits a statistically homogeneous distribution of phases. This assumption justifies the use of a periodic representative unit cell and enables the derivation of effective macroscopic properties.

(iii) Local thermodynamic stability. Each phase possesses a symmetric, bounded and strictly coercive elastic tensor, together with strictly positive transport coefficients. These properties ensure the coercivity of the variational formulation and guarantee the existence and uniqueness of weak solutions.

(iv) Regularity of constitutive parameters. All material parameters (elastic moduli, diffusion coefficients, kinetic constants) are assumed bounded and measurable, belonging to $L^{\infty}(\Omega)$. This regularity ensures stability of the homogenization process and prevents pathological behaviour in the limit problem.

(v) Linear elasticity and small strains. Under service conditions of cement-based structures, deformations remain sufficiently small to justify the linearized strain tensor and a linear elastic constitutive law.

These hypotheses constitute the minimal mathematical conditions required to derive the effective behaviour of the composite material.

3.2. Hierarchical Composite Medium

Let $\Omega \subset \mathbb{R}^3$ be a bounded open domain with Lipschitz boundary, representing the reference configuration of the cementitious material. The medium is described

as a heterogeneous multiphase composite composed of three principal constituents $\mathcal{I}=\{\text{C–S–H}, CH, GP\}$, where C-S-H denotes the calcium-silicate-hydrate gel, CH portlandite, and GP ground recycled glass powder. The macroscopic domain is decomposed into a measurable partition $\Omega=\bigcup_{\alpha\in\mathcal{I}}\Omega_\alpha$, $\Omega_\alpha\cap\Omega_\beta=\varnothing\ \ (\alpha\neq\beta)$, which defines the volumetric fractions $\phi_\alpha=\frac{|\Omega_\alpha|}{|\Omega|}$, $\sum_{\alpha\in\mathcal{I}}\phi_\alpha=1$.

The microstructure is assumed to be generated by a periodic unit cell $Y=(0,\,1)^3$, itself decomposed into subdomains Y_α associated with each phase. The microscopic configuration is obtained by the scaling $y=\frac{x}{\varepsilon}$, $0<\varepsilon\ll 1$, which induces the phase domains $\Omega_\alpha^\varepsilon=\{x\in\Omega\mid x/\varepsilon\in Y_\alpha\}$. This periodic hierarchical structure provides the analytical setting required for the rigorous application of homogenization techniques to derive effective properties at the macroscopic scale [18].

3.3. Intrinsic Properties of the Phases

Each phase is assumed locally homogeneous and isotropic, so that its mechanical behaviour is characterized by the fourth-order elasticity tensor $\mathbb{C}_\alpha=\lambda_\alpha\mathbf{I}\otimes\mathbf{I}+2\mu_\alpha\mathbf{I}_s$, where λ_α and μ_α are the Lamé coefficients, bijectively related to the Young's modulus E_α and Poisson's ratio ν_α. For the C-S-H phase, nanoindentation and microindentation experiments typically report $E_{\text{C-S-H}}\approx 20$ - 30 GPa for gels with porosities comparable to those of hardened cement paste, which we adopt as initial bounds for calibration.

In addition to mechanical parameters, each phase is endowed with a vector of intrinsic physico-chemical properties, $\mathbf{p}_\alpha=(\rho_\alpha, D_\alpha, \kappa_\alpha, S_\alpha)$, where ρ_α denotes the density, D_α the intrinsic diffusion coefficient, κ_α the permeability, and S_α the internal specific surface area. Orders of magnitude for D_α and κ_α are chosen in agreement with measured diffusion coefficients (~10^{-12} m²/s) and permeabilities (~10^{-18} - 10^{-16} m²) in hydrated cement pastes, and are refined in Section 5.

Under the hypotheses of local homogeneity, isotropy and energetic convexity, the families $\{\mathbb{C}_\alpha\}_\alpha$ and $\{\mathbf{p}_\alpha\}_\alpha$ define an admissible material parameter set for the homogenization procedure, ensuring the existence of effective macroscopic properties that remain symmetric, coercive and thermodynamically consistent [18] [19].

3.4. Morphological Parameters of Recycled Glass

The morphology of the recycled glass phase is described by a particle size distribution defined on an admissible size space $\mathcal{D}\subset\mathbb{R}_+$, with probability density $f_g(d)$ satisfying $\int_{\mathcal{D}} f_g(d)\,\mathrm{d}d=1$. The volumetric fraction of glass powder is $\phi_g=\frac{|\Omega_{GP}|}{|\Omega|}$, $0<\phi_g<\phi_{\text{crit}}$, where ϕ_{crit} denotes an upper bound imposed by

packing and workability constraints.

The specific surface area of the glass particles is defined as $S_g = \frac{1}{|\Omega_{GP}|}$ $\int_{\mathcal{D}} A(d)n(d)\mathrm{d}d$ where $A(d)$ denotes the surface of a particle of diameter d and $n(d)$ the associated number density. For approximately equiaxed particles, this yields the scaling relation $S_g \sim \int_{\mathcal{D}} d^{-1} f_g(d)\mathrm{d}d$, which makes explicit the increase of specific surface area as the particle size decreases. This parameter plays a central role in the pozzolanic reaction kinetics, since smaller glass particles (with larger S_g) exhibit significantly higher reactivity in alkaline media [19] [20].

3.5. Reaction Mechanism and Kinetic Law

The pozzolanic reaction between glass powder and portlandite is modelled as an irreversible first-order process with respect to the portlandite concentration, consistently with experimental observations on CH-glass systems. Let $C_{CH}(x,t)$ denote the molar concentration of portlandite; its evolution is governed by $\partial_t C_{CH}(x,t) = -k_p S_g C_{CH}(x,t)$, where $k_p > 0$ is the reaction rate constant and S_g the effective specific surface area of glass introduced in Section 2. The explicit solution $C_{CH}(x,t) = C_{CH}^0(x)\exp(-k_p S_g t)$ ensures positivity of concentrations and a strictly monotonic depletion of portlandite over time, in line with classical descriptions of pozzolanic activity.

3.6. Microstructural Evolution and Transport Coupling

The consumption of portlandite leads to the formation of secondary C-S-H phases and, consequently, to a progressive densification of the microstructure, which we describe through the connected porosity $\phi_p(x,t)$. We assume that ϕ_p is a strictly decreasing function of the local portlandite concentration, $\phi_p(x,t) = \Phi(C_{CH}(x,t))$, $\Phi'(s) < 0$, so that chemical consumption of C_{CH} directly translates into porosity reduction [20] [21].

The resulting evolution of ϕ_p modulates the effective transport properties, written as $k_{\text{eff}}(\phi_p) = \Psi_k(\phi_p)$, $D_{\text{eff}}(\phi_p) = \Psi_D(\phi_p)$, where Ψ_k and Ψ_D are decreasing functions calibrated from durability tests. Experimental data for dense cementitious materials typically yield apparent diffusion coefficients in the range $D_{\text{eff}} \sim 10^{-12}$ - $10^{-11}\ \mathrm{m^2/s}$, which we use as initial orders of magnitude for the identification of $D_{\text{eff}}(\phi_p)$ in the numerical section.

3.7. Coupled Chemo-Transport Mechanical System

The multiphysical behaviour of the cementitious composite is described at the structural scale by a coupled system of partial differential equations, which combines chemical kinetics, microstructural evolution, transport phenomena, and

mechanical response [16].

Let $C_{CH}:\Omega\times[0,T]\to\mathbb{R}_+$, $\phi_p:\Omega\times[0,T]\to[0,1]$, $c:\Omega\times[0,T]\to\mathbb{R}$, $\mathbf{u}:\Omega\times[0,T]\to\mathbb{R}^3$ denote, respectively, the portlandite concentration, connected porosity, diffusing species concentration, and displacement field. The evolution of these fields is governed by the coupled system

$$\begin{cases} \partial_t C_{CH}(x,t) = -k_p S_g(x) C_{CH}(x,t), & \text{in } \Omega\times(0,T], \\ \partial_t \phi_p(x,t) = \Phi'\big(C_{CH}(x,t)\big)\partial_t C_{CH}(x,t), & \text{in } \Omega\times(0,T], \\ \partial_t c(x,t) = \nabla\cdot\Big(D_{\text{eff}}\big(\phi_p(x,t)\big)\nabla c(x,t)\Big) + f(x,t), & \text{in } \Omega\times(0,T], \\ -\nabla\cdot\Big(\mathbb{C}^{\text{hom}}\big(\phi_p(x,t)\big):\varepsilon\big(\mathbf{u}(x,t)\big)\Big) = \mathbf{n}|, & \text{in } \Omega\times(0,T], \end{cases} \tag{1}$$

supplemented by the initial and boundary conditions

$$\begin{aligned} &C_{CH}(x,0) = C_{CH}^0(x), \quad c(x,0) = c^0(x), \quad \mathbf{u}(x,0) = \mathbf{0}, \\ &\mathbf{u}|_{\partial\Omega_D} = \mathbf{0}, \quad \Big(\mathbb{C}^{\text{hom}}\big(\phi_p\big)\varepsilon(\mathbf{u})\Big)\cdot\mathbf{n}|_{\partial\Omega_N} = \mathbf{t}_N, \\ &c|_{\partial\Omega_c} = c_D, \quad \Big(D_{\text{eff}}\big(\phi_p\big)\nabla c\Big)\cdot\mathbf{n}|_{\partial\Omega_f} = q_N. \end{aligned}$$

Here, $k_p>0$ is the pozzolanic kinetic constant, S_g the effective specific surface area of glass, Φ a strictly decreasing porosity-chemistry law, D_{eff} the effective diffusion coefficient typically in the range 10^{-12} - 10^{-11} m^2/s for chloride in dense concretes [22] [23], and $\mathbb{C}^{\text{hom}}$ the homogenized elastic tensor depending on ϕ_p.

Analytical properties. Under the hypotheses that:

- the functions S_g, Φ, and D_{eff} are bounded and Lipschitz-continuous with respect to their arguments,
- the homogenized tensor $\mathbb{C}^{\text{hom}}\big(\phi_p\big)$ is symmetric, uniformly coercive and bounded for all admissible $\phi_p\in[0,1]$,
- the initial and boundary data are smooth enough and compatible with the constraints, system (1) is *well-posed* in the sense of Hadamard, *i.e.* it admits a unique solution that depends continuously on the data in appropriate Sobolev spaces. This structure is consistent with standard parabolic-elliptic chemo-mechanical systems analysed in the literature.

More precisely:

- The kinetic equation for C_{CH} admits an explicit exponential solution, which preserves non-negativity of the portlandite concentration for all $t>0$.
- Since $\Phi'<0$ and $\partial_t C_{CH}\le 0$, the porosity ϕ_p remains in $[0,1]$ and decreases monotonically, reflecting microstructural densification.
- The diffusion equation for c with positive $D_{\text{eff}}\big(\phi_p\big)$ satisfies a maximum principle, ensuring that the concentration remains within physically admissible bounds.
- The mechanical equilibrium problem remains coercive for any admissible ϕ_p, which guarantees uniqueness and stability of the displacement field $\mathbf{u}$.

The present formulation implements a one-way chemo-mechanical coupling in which microstructural changes, encoded through ϕ_p, modulate stiffness and permeability via $\mathbb{C}^{\text{hom}}\left(\phi_p\right)$ and $D_{\text{eff}}\left(\phi_p\right)$, while remaining compatible with standard finite element spaces and stable time-integration schemes (e.g. semi-implicit or operator-splitting), whose numerical implementation and calibration of k_p, S_g, $D_{\text{eff}}\left(\phi_p\right)$, and $\mathbb{C}^{\text{hom}}\left(\phi_p\right)$ are detailed in Section 5.

4. Multiphysics and Multiscale Modeling of the Cementitious Composite

This section presents the theoretical and multiscale framework used to model the coupled chemo-microstructural-transport-mechanical behaviour of cementitious composites incorporating recycled glass. The formulation states the working hypotheses, identifies the parameters to be calibrated, and prepares the ground for the numerical implementation described in Section 5.

4.1. Mechanical Modeling and Multiscale Coupling

We work under the assumption of small, infinitesimal deformations and introduce a homogenized elasticity tensor $\mathbb{C}^{\text{eff}}:[0,\,1]\to\mathcal{L}\left(\mathbb{R}^{3\times3}_{\text{sym}},\,\mathbb{R}^{3\times3}_{\text{sym}}\right)$, which depends on the connected porosity ϕ_p. The tensor $\mathbb{C}^{\text{eff}}\left(\phi_p\right)$ is assumed Lipschitz-continuous and uniformly strictly elliptic, ensuring mechanical stability at all admissible porosities. The Cauchy stress field then satisfies the linear constitutive relation $\boldsymbol{\sigma}\left(\mathbf{x},t\right)=\mathbb{C}^{\text{eff}}\left(\phi_p\left(\mathbf{x},t\right)\right):\boldsymbol{\varepsilon}\left(\mathbf{u}\left(\mathbf{x},t\right)\right)$, $\boldsymbol{\varepsilon}\left(\mathbf{u}\right):=\frac{1}{2}\left(\nabla\mathbf{u}+\nabla\mathbf{u}^{\top}\right)$, together with suitable boundary conditions.

Key hypotheses for the multiscale mechanical model.

1) *Homogeneity at the mesoscale:* the material is statistically homogeneous at the scale of representative volume elements (RVE).
2) *Separation of scales:* microstructural features (porosity, glass inclusions) are much smaller than the macroscopic structural domain.
3) *Regularity of coefficients:* $\mathbb{C}^{\text{eff}}\left(\phi_p\right)$ is bounded, Lipschitz-continuous and strictly positive definite for all $\phi_p\in[0,1]$.

The microstructure evolution is described by the connected porosity $\phi_p:\Omega\times[0,T]\to[0,1]$, assumed to be a strictly decreasing function of the local molar concentration of portlandite C_{CH} via a smooth mapping $\Phi\in C^1\left(\mathbb{R}_+;[0,1]\right)$: $\phi_p\left(\mathbf{x},t\right)=\Phi\left(C_{CH}\left(\mathbf{x},t\right)\right)$, $\frac{\mathrm{d}\Phi}{\mathrm{d}C_{CH}}(s)<0\quad\forall s>0$. Consequently, $\frac{\partial\phi_p}{\partial t}=\Phi'\left(C_{CH}\right)\frac{\partial C_{CH}}{\partial t}<0$, which guarantees a monotone and irreversible decrease of porosity, consistent with progressive C-S-H formation and microstructural densification.

Transport processes.

The diffusion of aggressive species $c:\Omega\times[0,T]\to\mathbb{R}_+$ is governed by

$\frac{\partial c}{\partial t} = \nabla \cdot \left(D_{\text{eff}} \left(\phi_p \right) \nabla c \right) + f$, where $D_{\text{eff}} : [0,1] \to \mathbb{R}_+^*$ is a strictly decreasing, Lipschitz-continuous function of ϕ_p. In dense cementitious materials, typical orders of magnitude are $D_{\text{eff}} \sim 10^{-12}$ - $10^{-11}\ \text{m}^2/\text{s}$ for ionic species such as chlorides, which we adopt as initial bounds for calibration.

4.2. Chemical Kinetics and Multiscale Coupling

The local evolution of portlandite $C_{CH} : \Omega \times [0,T] \to \mathbb{R}_+$ is modelled as an irreversible first-order process with respect to C_{CH}, $\frac{\partial C_{CH}}{\partial t} = -k_p S_g \left(\mathbf{x}, t \right) C_{CH}$, where $k_p > 0$ is the kinetic rate constant and S_g the effective specific surface area of glass introduced in Section 2. Experimental studies on pozzolanic systems suggest typical ranges of k_p between about 10^{-5} and $10^{-3}\ \text{s}^{-1}$, which are refined during calibration for glass-CH systems [17] [21].

The specific surface S_g is taken inversely proportional to a characteristic particle size d_g, which evolves according to $\frac{\partial d_g}{\partial t} = -\mathcal{F}\left(C_{CH}, \boldsymbol{\varepsilon}\left(\mathbf{u} \right), d_g \right)$, where $\mathcal{F}$ is a Lipschitz-continuous function encoding chemo-microstructural mechanical feedback. In the present work, and for service stress levels, the dependence of $\mathcal{F}$ on $\boldsymbol{\varepsilon}\left(\mathbf{u} \right)$ is kept parametric, so that chemical kinetics primarily drive microstructural changes.

Fully coupled system. The resulting multiphysics–multiscale problem reads

$$\begin{cases} \dfrac{\partial C_{CH}}{\partial t} = -k_p S_g C_{CH}, \\ \dfrac{\partial d_g}{\partial t} = -\mathcal{F}\left(C_{CH}, \boldsymbol{\varepsilon}\left(\mathbf{u} \right), d_g \right), \\ \dfrac{\partial \phi_p}{\partial t} = \Phi'\left(C_{CH} \right) \dfrac{\partial C_{CH}}{\partial t}, \qquad \left(\mathbf{x}, t \right) \in \Omega \times \left(0, T \right], \\ \dfrac{\partial c}{\partial t} = \nabla \cdot \left(D_{\text{eff}} \left(\phi_p \right) \nabla c \right) + f, \\ -\nabla \cdot \left(\mathbb{C}^{\text{eff}} \left(\phi_p \right) : \boldsymbol{\varepsilon}\left(\mathbf{u} \right) \right) = \mathbf{0}, \end{cases}$$

complemented with initial and boundary conditions specified in Section 3. Under the regularity and coercivity assumptions stated above, this system is well-posed in appropriate Sobolev spaces and satisfies positivity, maximum-principle and stability properties consistent with the physics of the problem.

Parameters to calibrate. The following quantities are identified from experiments and literature data:

- chemical parameters: k_p (kinetic rate), S_g (specific surface), $\Phi\left(C_{CH} \right)$ (porosity-chemistry mapping), and $\mathcal{F}$ (granulometry evolution law);
- transport parameter: $D_{\text{eff}} \left(\phi_p \right)$, with initial bounds 10^{-12} - $10^{-11}\ \text{m}^2/\text{s}$ for dense matrices;
- mechanical parameter: $\mathbb{C}^{\text{eff}} \left(\phi_p \right)$, whose components correspond to effective

Young's moduli typically ranging from about 10 to 40 GPa for cement paste and concrete, depending on porosity and glass content.

Numerical implementation. The numerical solution strategy for this coupled problem discretization choices, time integration schemes (e.g. staggered or operator-splitting approaches), and parameter identification procedures is presented in Section 5, together with validation against experimental benchmarks.

5. Theoretical Analysis and Results

Let us consider the mappings $E_{\text{eff}}, D_{\text{eff}} : [0,\ \phi_{\text{crit}}] \to \mathbb{R}_+$, of class C^2, representing respectively the effective Young's modulus and the effective diffusivity as functions of the recycled glass volume fraction ϕ_g, with $\phi_{\text{crit}} > 0$ bounding the validity domain of the multiphysics model.

Theorem 1 (Existence and uniqueness of an optimal glass fraction) Assume that, for all $\phi_g \in (0, \phi_{\text{crit}})$, $E'_{\text{eff}}(\phi_g) > 0$, $E''_{\text{eff}}(\phi_g) < 0$, $D'_{\text{eff}}(\phi_g) < 0$, $D''_{\text{eff}}(\phi_g) > 0$, and let $(\alpha, \beta) \in \mathbb{R}_+^{*2}$. Define $F(\phi_g) := \alpha E_{\text{eff}}(\phi_g) - \beta D_{\text{eff}}(\phi_g)$, $\phi_g \in [0, \phi_{\text{crit}}]$. Suppose furthermore that $\lim_{\phi_g \to 0^+} F'(\phi_g) > 0$ and $\lim_{\phi_g \to \phi_{\text{crit}}^-} F'(\phi_g) < 0$. Then there exists a unique $\phi_g^{\text{opt}} \in (0, \phi_{\text{crit}})$ such that $F'(\phi_g^{\text{opt}}) = 0$ and $F''(\phi_g^{opt}) < 0$, so that ϕ_g^{opt} is the unique global maximizer of F on $[0, \phi_{\text{crit}}]$, representing the optimal compromise between mechanical reinforcement and diffusivity reduction.

Proof. We first consider the second derivative of F. For every $\phi_g \in (0, \phi_{\text{crit}})$, $F''(\phi_g) = \alpha E''_{\text{eff}}(\phi_g) - \beta D''_{\text{eff}}(\phi_g)$. By assumption, we have $E''_{\text{eff}}(\phi_g) < 0$ and $D''_{\text{eff}}(\phi_g) > 0$, with $\alpha, \beta > 0$. Hence $F''(\phi_g) = \alpha E''_{\text{eff}}(\phi_g) - \beta D''_{\text{eff}}(\phi_g) < 0$ $\forall \phi_g \in (0, \phi_{\text{crit}})$. This shows that F is strictly concave on $(0, \phi_{\text{crit}})$. Since $F \in C^2([0, \phi_{\text{crit}}])$, this strict concavity extends to the closed interval $[0, \phi_{\text{crit}}]$.

We now turn to the first derivative, $F'(\phi_g) = \alpha E'_{\text{eff}}(\phi_g) - \beta D'_{\text{eff}}(\phi_g)$. The inequality $F'' < 0$ implies that F' is strictly decreasing and continuous on $(0, \phi_{\text{crit}})$. By the boundary assumptions, $\lim_{\phi_g \to 0^+} F'(\phi_g) > 0$ and $\lim_{\phi_g \to \phi_{\text{crit}}^-} F'(\phi_g) < 0$. By continuity of F' and the intermediate value theorem, there exists at least one $\phi_g^{\text{opt}} \in (0, \phi_{\text{crit}})$ such that $F'(\phi_g^{\text{opt}}) = 0$ [18].

Because F' is strictly decreasing, this critical point is necessarily unique: if $\phi_1, \phi_2 \in (0, \phi_{\text{crit}})$ both satisfied $F'(\phi_1) = F'(\phi_2) = 0$, then we would have $\phi_1 = \phi_2$. Thus there exists a unique $\phi_g^{\text{opt}} \in (0, \phi_{\text{crit}})$ with $F'(\phi_g^{\text{opt}}) = 0$. Finally, the strict concavity of F on $[0,\ \phi_{\text{crit}}]$ implies that any interior critical point is a strict global maximum. Therefore $F''(\phi_g^{\text{opt}}) < 0$ and $F(\phi_g^{\text{opt}}) = \max_{\phi_g \in [0, \phi_{\text{crit}}]} F(\phi_g)$, which completes the proof.

We illustrate the behaviour of the functional $F(\phi_g)$ and of its derivative $F'(\phi_g)$ in **Figure 3**. The upper panel displays the graph of $F(\phi_g)$ on $[0, \phi_{\text{crit}}]$;

one observes a single, well-defined global maximum attained at ϕ_g^{opt}, in full agreement with the existence and uniqueness result established in Theorem 1. This maximizer corresponds to the unique optimal compromise between the increase of the effective stiffness $E_{\mathrm{eff}}\left(\phi_g\right)$ and the decrease of the effective diffusivity $D_{\mathrm{eff}}\left(\phi_g\right)$.

The lower panel shows the derivative $F'\left(\phi_g\right)$. As expected from the strict concavity of F, the function F' is strictly decreasing and crosses the horizontal axis exactly once, at ϕ_g^{opt}, where $F'\left(\phi_g^{\mathrm{opt}}\right)=0$. The vertical dashed line passing through ϕ_g^{opt} and the horizontal dashed line at the level $F_{\max}:=F\left(\phi_g^{\mathrm{opt}}\right)$ highlight the one-to-one correspondence between the unique critical point of F and its maximal value.

This graphical representation is fully consistent with the theoretical framework developed in the previous subsection and provides an explicit, visually transparent illustration of the optimal recycled glass fraction predicted by the model, which is directly usable for the rational design of cementitious composites incorporating recycled glass.

6. Numerical Implementation and Results

In this section, we describe the numerical implementation of the coupled chemo-transport-mechanical model introduced above and present representative simulation results. The objectives are (i) to verify the qualitative behaviour predicted by the theoretical analysis, in particular the emergence of an optimal glass volume fraction ϕ_g^{opt}, and (ii) to illustrate the spatio-temporal interaction between chemical kinetics, microstructural evolution, transport, and effective stiffness.

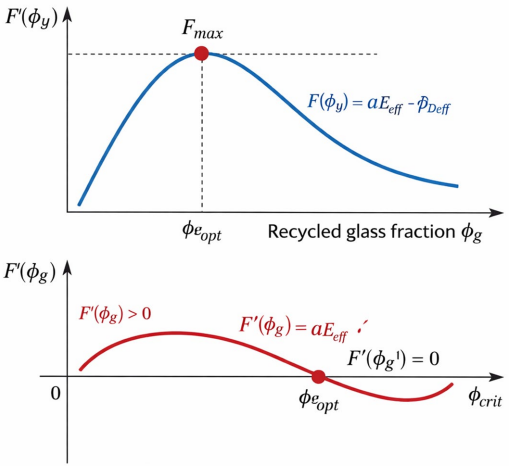

Figure 3. Visualization of the functional $F\left(\phi_g\right)=\alpha E_{\mathrm{eff}}-\beta D_{\mathrm{eff}}$ as a function of the recycled glass fraction ϕ_g. The top panel (blue curve) shows $F\left(\phi_g\right)$ with the unique global maximum ϕ_g^{opt} highlighted in red, while the bottom panel (red curve) illustrates the derivative $F'\left(\phi_g\right)$, crossing zero precisely at ϕ_g^{opt}. The dashed lines indicate the correspondence between the maximum value $F_{\max}$ and the optimal glass fraction.

6.1. Numerical Methods and Computational Setup

Spatial discretization. The coupled problem is solved using a standard finite element (FE) formulation on a bounded domain $\Omega \subset \mathbb{R}^d$ ($d = 2$ or 3), chosen here as a rectangular (or prismatic) domain representative of a structural element. The domain is discretized by conforming simplicial or quadrilateral/hexahedral elements. The displacement field $\mathbf{u}$ is approximated in a vector-valued H^1-conforming FE space (e.g. continuous P_1 or P_2 elements), while the scalar fields C_{CH}, c, and ϕ_p are approximated in scalar H^1-conforming FE spaces (continuous P_1 elements).

Temporal discretization. Time integration is performed on a uniform grid $0 = t_0 < t_1 < \cdots < t_N = T$ with time step Δt. The diffusion and reaction equations are advanced using a first-order backward Euler scheme (implicit in time), which is unconditionally stable for the linear terms. The kinetic equation for C_{CH} can, if desired, be integrated in closed form at the element or quadrature level, using the explicit solution

$$C_{CH}\left(x, t_{n+1}\right) = C_{CH}\left(x, t_n\right) \exp\left(-k_p S_g\left(x\right) \Delta t\right),$$

thus avoiding stiffness issues in the time discretization of the reaction term.

Solution strategy and tolerances. At each time step t_{n+1}, we adopt a staggered (partitioned) solution procedure:

1) Update C_{CH}^{n+1} from the kinetic law (explicit exponential update or implicit FE solve).

2) Update $\phi_p^{n+1} = \Phi\left(C_{CH}^{n+1}\right)$ and the effective coefficients $D_{\text{eff}}\left(\phi_p^{n+1}\right)$, $\mathbb{C}^{\text{eff}}\left(\phi_p^{n+1}\right)$.

3) Solve the diffusion problem for c^{n+1} with coefficient $D_{\text{eff}}\left(\phi_p^{n+1}\right)$.

4) Solve the quasi-static elasticity problem for $\mathbf{u}^{n+1}$ with tensor $\mathbb{C}^{\text{eff}}\left(\phi_p^{n+1}\right)$.

Each elliptic subproblem is solved by a preconditioned conjugate gradient or GMRES method with relative tolerance 10^{-8} on the residual norm. Nonlinearities (if any) in Φ, D_{eff}, or $\mathbb{C}^{\text{eff}}$ are treated explicitly in time at this stage; a fully implicit monolithic scheme could be implemented but is beyond the present scope [24].

Domain, boundary and initial conditions. Unless otherwise specified, Ω is taken as a unit square (2D) or unit cube (3D), $\Omega = \left(0,1\right)^d$, with:

- homogeneous Dirichlet boundary conditions for displacement on a portion $\partial\Omega_D$ (clamped boundary) and prescribed tractions $\mathbf{t}_N$ on $\partial\Omega_N = \partial\Omega \setminus \partial\Omega_D$;
- a prescribed concentration $c = c_D$ on an exposed boundary $\partial\Omega_c$ and homogeneous Neumann flux $\left(D_{\text{eff}} \nabla c\right) \cdot \mathbf{n} = 0$ on the remaining part $\partial\Omega_f$;
- initial conditions $C_{CH}\left(x,0\right) = C_{CH}^0\left(x\right)$, $\phi_p\left(x,0\right) = \Phi\left(C_{CH}^0\left(x\right)\right)$, $c\left(x,0\right) = 0$, and $\mathbf{u}\left(x,0\right) = \mathbf{0}$.

Parameter selection and calibration. The kinetic constant k_p, the porosity-chemistry law Φ, and the transport law $D_{\text{eff}}\left(\phi_p\right)$ are chosen in ranges compatible with experimental data on glass-CH systems and dense cementitious matrices,

then refined by matching reference measurements (e.g. CH depletion curves, diffusion tests, effective modulus). Similarly, the dependence of $\mathbb{C}^{\text{eff}}$ on ϕ_p is calibrated against effective stiffness values inferred from homogenization or from mechanical tests at different glass contents. The scalar weights $\alpha, \beta > 0$ entering the objective functional $F(\phi_g)$ are selected to reflect the relative importance assigned to stiffness and durability in a given design scenario.

6.2. Spatio-Temporal Evolution of Chemical and Microstructural Fields

Figure 4 shows representative snapshots of the portlandite concentration C_{CH} and the associated porosity field ϕ_p at three successive times. The depletion of C_{CH} progresses from the exposed boundary into the bulk, driven by the pozzolanic reaction and diffusion of aggressive species. Consistently with the assumed law $\phi_p = \Phi(C_{CH})$ with $\Phi' < 0$, the porosity decreases monotonically in regions where C_{CH} is consumed, illustrating the microstructural densification induced by the reaction.

6.3. Diffusive Transport in the Evolving Microstructure

Figure 5 displays the evolution of the diffusing species concentration c at the same time instants. The penetration front advances into the material, but its progression slows down as microstructural densification reduces the local effective diffusivity $D_{\text{eff}}(\phi_p)$. This behaviour is consistent with the strictly decreasing dependence of D_{eff} on ϕ_p and illustrates the feedback of chemical-microstructural changes on transport properties.

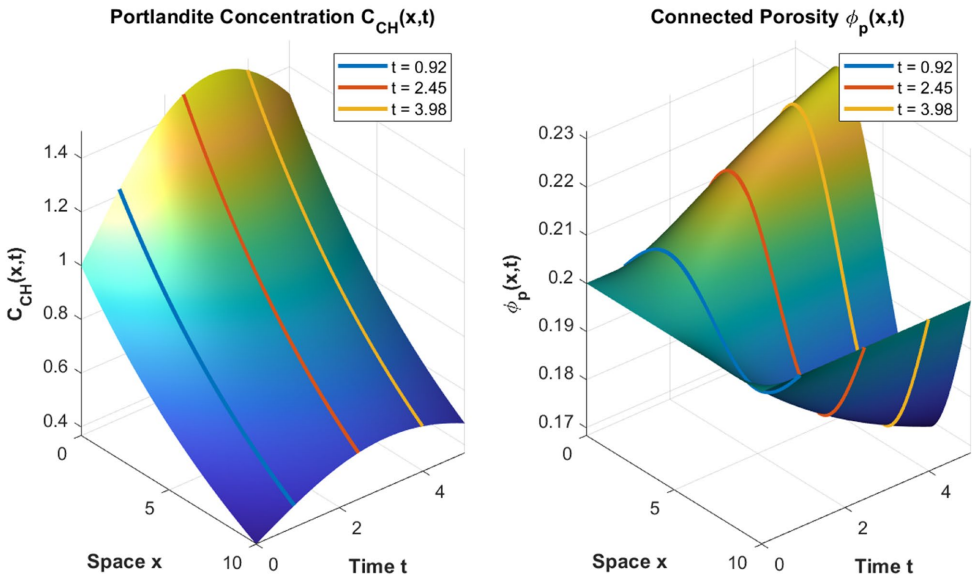

Figure 4. Spatio-temporal evolution of portlandite concentration $C_{CH}(x,t)$ (top row) and connected porosity $\phi_p(x,t)$ (bottom row) at three increasing times $t_1 < t_2 < t_3$.

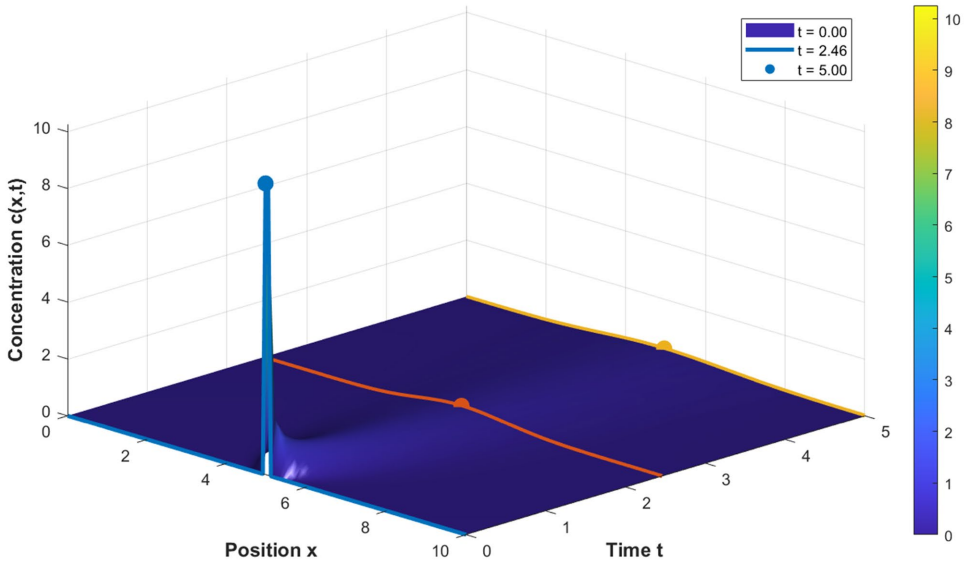

Figure 5. Concentration field $c(x,t)$ at times t_1, t_2, and t_3, highlighting the impact of the evolving porosity (and thus $D_{\text{eff}}(\phi_p)$) on the penetration depth of the diffusing species.

6.4. Effective Stiffness Degradation and Chemo-Mechanical Coupling

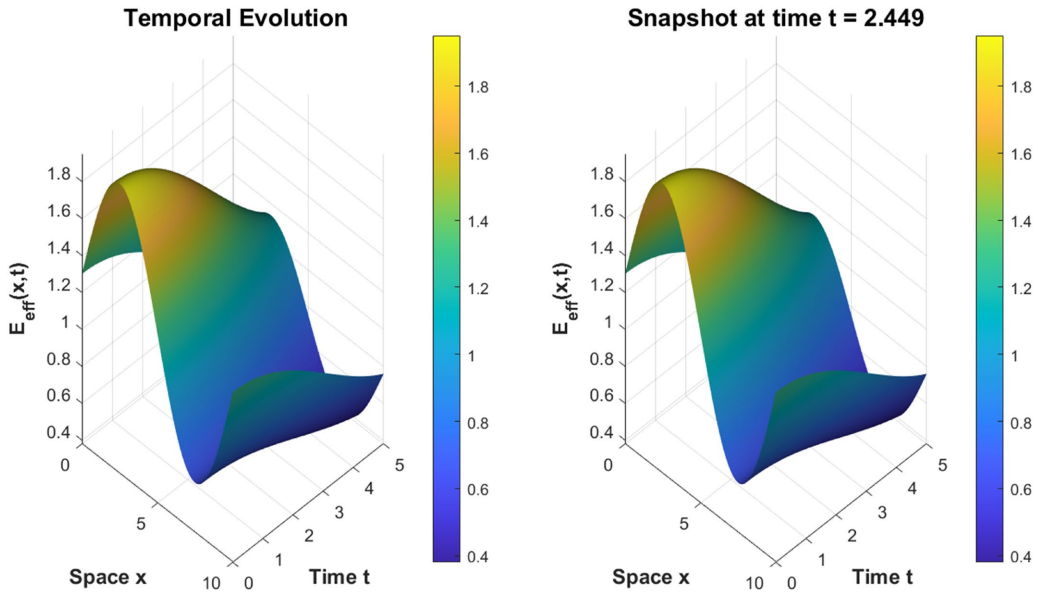

Figure 6. Temporal evolution of the volume-averaged effective Young's modulus $E_{\text{eff}}(t)$, together with the corresponding spatial distribution of $E_{\text{eff}}(x,t)$ at selected times.

The impact of the evolving microstructure on mechanical properties is summarized in Figure 6. The volume-averaged effective Young's modulus,

$$E_{\text{eff}}(t) = \frac{1}{|\Omega|}\int_{\Omega} E_{\text{eff}}\left(\phi_p(x,t)\right)\mathrm{d}x,$$

decreases over time as the chemical process and resulting porosity changes modify the local stiffness. Spatial maps of $E_{\text{eff}}(x,t)$ reveal that degradation is concentrated near the exposed boundary, where chemical attack and CH depletion are most pronounced. These results confirm the consistency of the chemo-mechanical coupling implemented in the model.

6.5. Numerical Evaluation of the Optimal Glass Volume Fraction

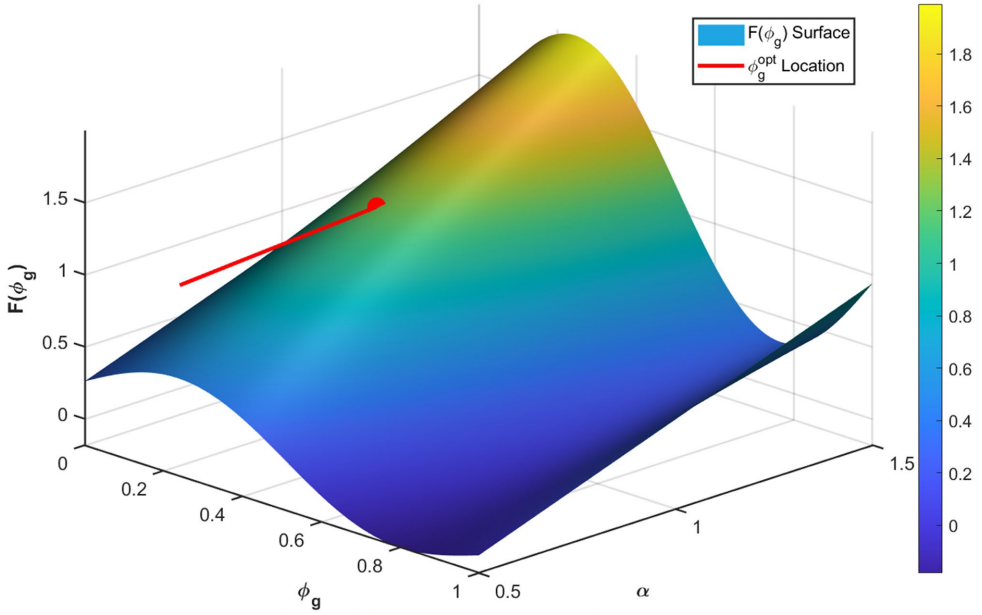

Figure 7. Graph of the objective functional $F(\phi_g)=\alpha E_{\text{eff}}(\phi_g)-\beta D_{\text{eff}}(\phi_g)$ and its derivative $F'(\phi_g)$, illustrating the unique optimal value ϕ_g^{opt} predicted by Theorem 1.

Figure 7 provides a numerical illustration of the theoretical result of Section. The upper panel shows a strictly concave profile of $F(\phi_g)$ on $[0,\ \phi_{\text{crit}}]$ with a single global maximum at ϕ_g^{opt}. The lower panel displays the corresponding derivative $F'(\phi_g)$, which is strictly decreasing and crosses zero only once, at the same value ϕ_g^{opt}, in agreement with the proof. This confirms, at the numerical level, the existence and uniqueness of an optimal glass fraction that achieves a balance between stiffness enhancement and diffusivity reduction.

6.6. Quantitative Insights from Multiphysics-Multiscale Numerical Simulations

The numerical experiments reported in this section consistently confirm the qualitative behaviour predicted by the theoretical framework and provide quantitative insight into the underlying mechanisms. In particular, they show that:

- the chemo-microstructural kinetics produce a spatially heterogeneous but monotone depletion of portlandite, accompanied by a progressive densification of the microstructure in the most reactive zones;

- the effective diffusivity is markedly reduced in regions where densification occurs, which significantly limits the penetration depth of aggressive species and thus enhances durability;
- the evolution of the effective stiffness is strongly coupled to the chemical and microstructural fields, leading to localized mechanical degradation that closely follows the zones of most intense chemical attack;
- the optimal recycled glass volume fraction ϕ_g^{opt}, established analytically, emerges clearly in the numerical evaluation of the functional $F\left(\phi_g\right)$, thereby corroborating the existence and uniqueness result at the computational level.

Taken together, these observations support the relevance and robustness of the proposed multiphysics-multiscale framework and underline its potential as a practical tool for the rational design and optimization of cementitious composites incorporating recycled glass.

7. Discussion

In this section, we interpret the significance of the numerical and theoretical results, critically assess the limitations of the current modeling framework, and outline several perspectives for future developments.

7.1. Interpretation of the Results

The simulations presented above are qualitatively consistent with reported trends on portlandite consumption, microstructural densification, and the associated evolution of transport properties in blended cementitious systems [4] [6] [7]. In particular, the numerically observed exponential-type depletion of C_{CH}, the monotone decrease of the connected porosity ϕ_p, and the reduction of the effective diffusivity $D_{\text{eff}}\left(\phi_p\right)$ are in line with the expected behaviour of pozzolanic reactions under diffusion-controlled exposure conditions. The spatial localization of stiffness degradation near exposed boundaries similarly reflects chemo-mechanical coupling mechanisms documented in durability studies of cement-based materials [4] [8].

More broadly, the results show that the fully coupled multiphysics-multiscale framework provides a coherent qualitative picture of the feedback loops between chemistry, microstructure, transport, and mechanics. The existence and uniqueness of an optimal recycled glass volume fraction ϕ_g^{opt}, established analytically and reproduced numerically through the functional $F\left(\phi_g\right)$, offer a clear theoretical basis for defining "optimal dosage" criteria in terms of stiffness durability trade-offs. Although the present simulations are not calibrated to a specific formulation, they supply a sound conceptual foundation for rational mix design in concretes incorporating recycled glass, under eco-efficient constraints.

7.2. Limitations of the Present Framework

The proposed model rests on several simplifying assumptions that must be kept

in mind when interpreting the results. First, the hypotheses of local homogeneity (in the sense of Hill) and strict separation of scales are essential for analytical homogenization and for the well-posedness of the multiscale problem, but they restrict direct applicability to materials with pronounced mesoscopic heterogeneities or to configurations where scale separation is questionable. Second, the mechanical response is described by small-strain linear elasticity, which is appropriate for service conditions but cannot capture cracking, damage, or other nonlinear phenomena that may arise under severe loading or long-term degradation [25].

Third, the kinetic and transport parameters (k_p , Φ, $D_{\text{eff}}\left(\phi_p\right)$, $\mathbb{C}^{\text{eff}}\left(\phi_p\right)$) have been selected within ranges compatible with the literature but have not yet been rigorously calibrated against a dedicated experimental data set for the specific glass-cement system considered. The present results should therefore be regarded as qualitative and illustrative rather than quantitative predictions for a particular composite. Finally, the assumption of a one-way coupling from chemistry and microstructure to mechanics (with no feedback of stress or damage on reaction rates and transport) constitutes an additional simplification that may need to be revisited for highly constrained, cracked, or strongly anisotropic systems.

7.3. Perspectives and Hybrid Approaches

Several extensions of the framework appear both natural and promising. On the physical side, incorporating explicit heterogeneities (aggregates, ITZ, defects) via stochastic or non-periodic microstructures, and relaxing the linear elastic assumption toward damage, fracture, or viscoelastic-viscoplastic models, would improve the representativeness of the simulations at the structural scale. Likewise, extending the model to fully coupled chemo-thermo-hydro-mechanical formulations would enable the analysis of more complex durability scenarios involving temperature, moisture transport, and multi-species interactions.

On the methodological side, hybrid strategies that combine the present mechanistic, interpretable model with data-driven or machine-learning components constitute an attractive direction. For example, physics-informed neural networks or surrogate models could be trained on high-fidelity numerical simulations to accelerate parametric studies, while preserving physical consistency through the governing equations. Conversely, experimental databases on glass-powder cementitious materials could be exploited to learn effective closure relations (for $D_{\text{eff}}\left(\phi_p\right)$, $\mathbb{C}^{\text{eff}}\left(\phi_p\right)$, or kinetic parameters), with the mechanistic framework providing structure and extrapolation capability. Finally, targeted experimental campaigns dedicated to parameter identification and validation would be crucial to move from qualitative agreement to quantitatively predictive simulations. Together, these perspectives point toward a hybrid, physics-informed and data-enriched framework for the design and optimization of eco-efficient, durable cementitious composites incorporating recycled glass.

8. Conclusion and Future Work

This study has introduced a mechanistic framework that systematically links recycled glass incorporation, microstructural evolution, transport properties, and effective mechanical response in cementitious composites. By combining the chemical kinetics of portlandite consumption, microstructure-informed transport and elasticity, and an optimization principle based on the functional $F\left(\phi_g\right)$, the model provides a coherent qualitative understanding of the stiffness-durability trade-offs induced by recycled glass powder. The theoretical analysis-particularly the existence and uniqueness of an optimal glass volume fraction ϕ_g^{opt}-offers a clear conceptual basis for rational mix design under eco-efficient constraints. Beyond its intrinsic predictive structure, the framework is naturally suited to serve as a physics-based prior in data-driven modeling. In transfer-learning or domain-adaptation settings, the governing equations and homogenization structure can be embedded as constraints or inductive biases within machine-learning architectures, guiding the learning process toward physically admissible regimes and improving extrapolation capabilities [26] [27]. Similarly, the homogenization operator and the effective laws $D_{\text{eff}}\left(\phi_p\right)$ and $\mathbb{C}^{\text{eff}}\left(\phi_p\right)$ can be approximated using interpretable surrogate models constructed via symbolic regression, explainable machine learning, or Kolmogorov-Arnold-type networks, which aim to recover closed-form relations while respecting known physical bounds [28] [29]. A key priority for future work is the design and execution of targeted experimental campaigns focused on cementitious composites with recycled glass. Such campaigns should provide time-resolved measurements of portlandite content, porosity, effective diffusivity, and effective Young's modulus for selected glass dosages under controlled environmental conditions. These data will be essential for calibrating the kinetic, transport, and mechanical parameters of the model, as well as for quantitative validation of the predicted curves $C_{CH}\left(t\right)$, $\phi_p\left(t\right)$, $D_{\text{eff}}\left(t\right)$, and $E_{\text{eff}}\left(t\right)$. In parallel, integrating the calibrated mechanistic model with physics-informed or hybrid surrogates (e.g., reduced-order models or neural operators constrained by the governing equations) will enable rapid parametric studies and multi-objective optimization across broader design spaces [27] [28]. This contribution establishes a solid theoretical and numerical foundation for the multiphysics-multiscale analysis of cementitious composites incorporating recycled glass. By explicitly linking mechanistic modeling, experimental calibration, and emerging physics-informed and explainable machine-learning strategies, it delineates a realistic and fertile roadmap for future research. The combination of these elements is expected to support the development of quantitatively reliable, computationally efficient, and environmentally responsible design tools for next-generation cement-based materials.

Acknowledgements

The authors thank the National Higher Polytechnic School and the University of

Douala for their support, as well as the laboratory staff and collaborators who contributed to the experimental and characterization work.

Conflicts of Interest

The authors declare no conflicts of interest regarding the publication of this paper.

References

[1] Broohm, A.A. (2003) Homogénéisation du comportement élastique des composites avec la prise en compte de l'endommagement. Ph.D. Thesis, Université Paul Verlaine-Metz. (in French) https://hal.univ-lorraine.fr/tel-01749841v1

[2] Chen, Y., Champenois, J.-B., Dangla, P., Granet, S., Lautru, J., Leclerc, A., *et al.* (2023) Investigation of Bituminized Waste Products Swelling Behavior Due to Water Uptake under Free Leaching Conditions: Experiments and Modeling. *International Journal for Numerical and Analytical Methods in Geomechanics*, **47**, 3351-3380. https://doi.org/10.1002/nag.3624

[3] Hepworth, D.G., Hobson, R.N., Bruce, D.M. and Farrent, J.W. (2000) The Use of Unretted Hemp Fibre in Composite Manufacture. *Composites Part A*: *Applied Science and Manufacturing*, **31**, 1279-1283. https://doi.org/10.1016/s1359-835x(00)00098-1

[4] Wang, W., Sain, M. and Cooper, P. (2006) Study of Moisture Absorption in Natural Fiber Plastic Composites. *Composites Science and Technology*, **66**, 379-386. https://doi.org/10.1016/j.compscitech.2005.07.027

[5] El Farissi, A. (2020) Prédiction de la durée d'utilisation des ouvrages en béton armé par une approche performantielle dans le cas de la corrosion induite par la carbonatation ou l'attaque des ions chlorure. Thèse de Doctorat, Université de La Rochelle. (in French)

[6] Voigt, W. (1889) Ueber die Beziehung zwischen den beiden Elasticitätsconstanten isotroper Körper. *Annalen der Physik*, **274**, 573-587. https://doi.org/10.1002/andp.18892741206

[7] Hill, R. (1965) A Self-Consistent Mechanics of Composite Materials. *Journal of the Mechanics and Physics of Solids*, **13**, 213-222. https://doi.org/10.1016/0022-5096(65)90010-4

[8] Sreekala, M.S. and Thomas, S. (2003) Effect of Fibre Surface Modification on Water-Sorption Characteristics of Oil Palm Fibres. *Composites Science and Technology*, **63**, 861-869. https://doi.org/10.1016/s0266-3538(02)00270-1

[9] Hoang, H. (2012) Modélisation du comportement et des couplages HMC des milieux poreux. Thèse de Doctorat, Université d'Orléans. https://theses.hal.science/tel-01622632

[10] Mori, T. and Tanaka, K. (1973) Average Stress in Matrix and Average Elastic Energy of Materials with Misfitting Inclusions. *Acta Metallurgica*, **21**, 571-574. https://doi.org/10.1016/0001-6160(73)90064-3

[11] Liuzzi, S., Sanarica, S. and Stefanizzi, P. (2017) Use of Agro-Wastes in Building Materials in the Mediterranean Area: A Review. *Energy Procedia*, **126**, 242-249. https://doi.org/10.1016/j.egypro.2017.08.147

[12] Fischer, S., Roman, I., Harel, H., Marom, G. and Wagner, H. (1981) Simultaneous Determination of Shear and Young's Moduli in Composites. *Journal of Testing and Evaluation*, **9**, 303-307. https://doi.org/10.1520/jte11520j

[13] Cichocki, F.R. and Thomason, J. L. (2002) Thermoelastic Anisotropy of a Natural

Fiber. *Composites Science and Technology*, **62**, 669-678. https://doi.org/10.1016/s0266-3538(02)00011-8

[14] Cherif, Z.E., Poilâne, C., Falher, T., Vivet, A., Ouail, N., Doudou, B.B., *et al.* (2013) Influence of Textile Treatment on Mechanical and Sorption Properties of Flax/Epoxy Composites. *Polymer Composites*, **34**, 1761-1773. https://doi.org/10.1002/pc.22580

[15] Huguet, S., Godin, N., Gaertner, R., Salmon, L. and Villard, D. (2002) Use of Acoustic Emission to Identify Damage Modes in Glass Fibre Reinforced Polyester. *Composites Science and Technology*, **62**, 1433-1444. https://doi.org/10.1016/s0266-3538(02)00087-8

[16] Marec, A., Thomas, J.H., Guerjouma, R.E. and Berbaoui, R. (2009) Investigation of Damage Mechanisms of composite Materials: Multivariable Analysis Based on Temporal and Wavelet Features Extracted from Acoustic Emission Signals. In: Leger, A., Deschamps, M. (Eds) *Ultrasonic Wave Propagation in Non Homogeneous Media*, Springer Proceedings in Physics, Vol 128. Springer, Berlin. https://doi.org/10.1007/978-3-540-89105-5_35

[17] de Groot, P.J., Wijnen, P.A.M. and Janssen, R.B.F. (1995) Real-Time Frequency Determination of Acoustic Emission for Different Fracture Mechanisms in Carbon/Epoxy Composites. *Composites Science and Technology*, **55**, 405-412. https://doi.org/10.1016/0266-3538(95)00121-2

[18] Friedrich, K. (1985) Microstructural Efficiency and Fracture Toughness of Short Fiber/Thermoplastic Matrix Composites. *Composites Science and Technology*, **24**, 145-157.

[19] Spahr, D.E., Friedrich, K., Schultz, J.M. and Bailey, R.S. (1990) Microstructure and Fracture Behaviour of Short and Long Fibre-Reinforced Polypropylene Composites. *Journal of Materials Science*, **25**, 4427-4439. https://doi.org/10.1007/bf00581104

[20] Woo, S. and Choi, N. (2007) Analysis of Fracture Process in Single-Edge-Notched Laminated Composites Based on the High Amplitude Acoustic Emission Events. *Composites Science and Technology*, **67**, 1451-1458. https://doi.org/10.1016/j.compscitech.2006.07.022

[21] Akil, H.M.D., Cheng, L.W., Ishak, Z.A.M., Bakar, A.A. and Abd Rahman, M.A. (2009) Water Absorption Study on Pultruded Jute Fibre Reinforced Unsaturated Polyester Composites. *Composites Science and Technology*, **69**, 1942-1948. https://doi.org/10.1016/j.compscitech.2009.04.014

[22] Mishra, S., Naik, J.B. and Patil, Y.P. (2000) The Compatibilising Effect of Maleic Anhydride on Swelling and Mechanical Properties of Plant-Fiber-Reinforced Novolac Composites. *Composites Science and Technology*, **60**, 1729-1735. https://doi.org/10.1016/s0266-3538(00)00056-7

[23] Thwe, M.M. and Liao, K. (2002) Effects of Environmental Aging on the Mechanical Properties of Bamboo-Glass Fiber Reinforced Polymer Matrix Hybrid Composites. *Composites Part A*: *Applied Science and Manufacturing*, **33**, 43-52. https://doi.org/10.1016/s1359-835x(01)00071-9

[24] Assarar, M., Scida, D., El Mahi, A., Poilâne, C. and Ayad, R. (2011) Influence of Water Ageing on Mechanical Properties and Damage Events of Two Reinforced Composite Materials: Flax-Fibres and Glass-Fibres. *Materials & Design*, **32**, 788-795. https://doi.org/10.1016/j.matdes.2010.07.024

[25] Joseph, P.V., Rabello, M.S., Mattoso, L.H.C., Joseph, K. and Thomas, S. (2002) Environmental Effects on the Degradation Behaviour of Sisal Fibre Reinforced Polypropylene Composites. *Composites Science and Technology*, **62**, 1357-1372. https://doi.org/10.1016/s0266-3538(02)00080-5

[26] Kempf, M., Skrabala, O. and Altstädt, V. (2014) Acoustic Emission Analysis for Characterisation of Damage Mechanisms in Fibre Reinforced Thermosetting Polyurethane and Epoxy. *Composites Part B*: *Engineering*, **56**, 477-483. https://doi.org/10.1016/j.compositesb.2013.08.080

[27] Nakka, R., Harursampath, D. and Ponnusami, S.A. (2023) A Generalised Deep Learning-Based Surrogate Model for Homogenisation Utilising Material Property Encoding and Physics-Based Bounds. *Scientific Reports*, **13**, Article No. 9079. https://doi.org/10.1038/s41598-023-34823-3

[28] Gommers, B., Verpoest, I. and Van Houtte, P. (1998) Determination of the Mechanical Properties of Composite Materials by Tensile Tests. Part II: Strength Properties. *Journal of Composite Materials*, **32**, 102-122. https://doi.org/10.1177/002199839803200201

[29] Liu, Z., Wang, Y., Vaidya, S., Ruehle, F., Halverson, J., Soljačić, M., Hou, T.Y. and Tegmark, M. (2024) KAN: Kolmogorov-Arnold Networks. arXiv:2404.19756.